14ASTC-0084

Optimal Control Allocation for Electric Aircraft Taxi Systems: a Preliminary Study

Author, co-author (Do NOT enter this information. It will be pulled from participant tab in MyTechZone)

Affiliation (Do NOT enter this information. It will be pulled from participant tab in MyTechZone)

Abstract

Demonstrators and research projects about electric aircraft taxi systems testify the current interest in low- or zero-emission ground propulsion technologies to lower the overall fuel consumption and emissions of commercial flights. Electric motors fitted in the main landing gears are one of the most promising layouts for these systems especially for narrow-body commercial aircraft. From a control theory point of view, the aircraft on ground becomes an over-actuated plant through adoption of this technology, i.e. a commanded ground trajectory can be reached through different combinations of actuator efforts. A strategy is required to choose the most suitable of these combinations in order to reach the best efficiency. This work aims to investigate a strategy for an optimal control allocation during path-following of prescribed ground trajectories. While the most obvious contributor to the optimizing cost function is energy efficiency, other aspects need to be considered such as the thermal behavior of the electric motors, the availability of energy storage systems resulting in a certain possible amount of regenerative braking, and other technical and normative constraints. Preliminary simulations of trajectory tracking based on the presented concept are shown.

Introduction

The standard way of performing aircraft ground operations has a poor energetic efficiency. Whenever commercial aircraft need to move on ground under their own power, their jet engines mostly run at idle, which is a very inefficient condition as far as fuel consumption and emissions are concerned. Carbon monoxide (CO) emissions are particularly high because of incomplete fuel combustion, [1] whereas more than half of the nitrogen oxides (NO_x) measured in a large airport area like London Heathrow over a year are ascribed to aircraft ground operations. [2] Furthermore, the idle thrust is too large in most taxiing conditions beside acceleration. The pilot is forced to use the brakes repeatedly against the idle thrust while taxiing, resulting in brake wear.

Pollution problems will increase with the predicted growth in air traffic. According to [3], the demanded Revenue Passenger Kilometers (RPK) are predicted to grow by 137% in Europe, by 130% in North America, and by more than 200% in the rest of the world over the period 2005-2025, while at the same time, the overall rise in number of IFR flights in Europe might be as high as 150% under best assumptions. The increased traffic obviously affects airport congestion. Within only four years from 2003 to 2007, the average taxi-out and taxi-in times in US airports increased by 11% and 9% respectively. [4]

In view of the still unused potential for efficiency improvement in taxi, a number of solutions have been proposed and investigated. Although the practice of one-engine taxiing – i.e. using only a subset of the jet engines for ground operations with reduction of the overall idle thrust and an inherent efficiency increase – would be available immediately on today's aircraft, technical and procedural concerns [5,6] regularly cause airlines to favor the standard all-engine taxi procedure.

Dispatch towing has also been proposed, consisting in towing the aircraft with an external tractor beyond pushback during all the taxi phase. While being a very interesting solution in theory, some aspects need to be considered in practice. The power of the tractors should be sensibly higher than today's pushback tugs in order to reach appropriate taxi speeds. The larger driving forces require a redesign of the towbar and the connecting devices on the aircraft. Because flight regulations require that pilot should be in full command of the aircraft during taxi, dispatch towing should feature a remote control of the tractor by the pilot to make it compliant. Finally, a large number of tractors traveling in airport areas such as taxiways will require major infrastructural and procedural changes that the stakeholders might not be ready or willing to undertake.

Many airframers and research institutions have focused on on-board driving systems for ground operations. While the specific layouts and specifications differ, all of these systems feature one or more electric motors driving the landing gear wheels. The reader is referred to [7] for a description of recent projects

on this field. Most of those projects adopt a layout with an even number of electric motors fitted into the main landing gears. Among the reasons for this choice, the vertical load is higher on the main gear wheels due to the aircraft mass distribution between the nose and the main gear, resulting in a better traction in low-grip conditions. Moreover, it is easier to realize a sufficiently powerful system by means of several motors. Finally, the redundancy increases the system reliability. From a control theory point of view, this forms an overactuated system: commanded longitudinal speeds and yaw rates can be reached through different combinations of actuator efforts, i.e. electric motors, conventional carbon brakes, and nose gear steering. For this reason, optimal allocation methods are required in order to choose the most suitable distribution of efforts. While the energetic efficiency will be the main goal of the optimized control, other constraints also need to be considered: a given degree of precision in following a prescribed trajectory should be guaranteed; technical aspects such as the thermal behavior of the electric motors should be accounted for, e.g. the motors may be driven more gently at the expense of performance if they risk overheating.

In this paper, we analyze a strategy to realize optimal path following algorithms for driving an aircraft with such a ground driving system along a ground trajectory. This is meant to be a first step towards the realization of real-time optimal control systems based on model predictive algorithms. We consider a vehicle equipped with electric motors on the landing gears and an energy storage system that makes regenerative braking possible. A primary source of energy for the ground driving system is assumed always available whenever the storage system cannot supply the needed power; the technical details of this energy source are not dealt with in this paper. In practice, the Auxiliary Power Unit (APU) is often used as primary energy source in the related research projects on these systems. After obtaining the mathematical model of the vehicle considered, we define the optimal control problem considering relevant technical constraints and limitations. Afterwards, we present some optimization results based on simplifying assumptions. We conclude the paper with some final remarks and an outlook.

Mathematical model

The vehicle represented in Figure 1 will be used as reference for deriving the equations of motion of an aircraft on ground. In order to simplify the problem, the model features one wheel per landing gear. Each main gear wheel is assumed to be connected to one electric motor and one standard carbon brake, thus being able to provide both a driving and a braking moment. The nose gear wheel has a steering system and spins freely, i.e. its driving moment is assumed zero at all times. Vertical dynamics are neglected as well as the main jet engines.

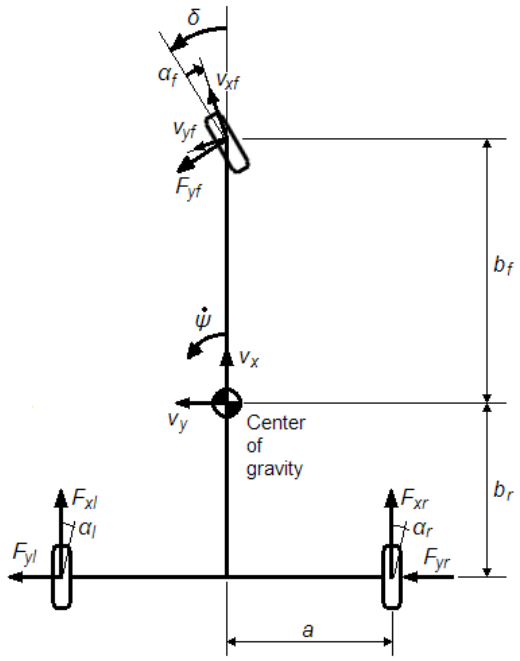

Figure 1. Model of an aircraft on ground.

The equations of motion are as follows:

$$\begin{aligned} m\left(\dot{v}_x - \dot{\psi} v_y\right) &= -F_{yf}\sin\delta + F_{xl} + F_{xr} - F_{res} \\ m\left(\dot{v}_y + \dot{\psi} v_x\right) &= F_{yf}\cos\delta + F_{yl} + F_{yr} \\ J_z\ddot{\psi} &= b_f F_{yf}\cos\delta - b_r\left(F_{yl} + F_{yr}\right) + a\left(-F_{xl} + F_{xr}\right) \end{aligned} \tag{1}$$

where:

- m and J_z are the aircraft mass and moment of inertia around the vertical body axis (part of a body-fixed reference frame with origin in the aircraft center of gravity);
- v_x and v_y are the longitudinal and lateral speed along in the body-fixed reference frame;
- $\dot{\psi}$ is the yaw rate;
- $F_{..}$ are the forces exerted by the tires in longitudinal (tangential) and lateral (axial) direction with regard to a wheel-fixed reference system. The first letter in the subscript is either x or y and refers to the longitudinal resp. lateral direction, whereas the second letter stands for **f**ront, **l**eft (main), or **r**ight (main) wheel;
- F_{res} is a term subsuming all the resistances experienced during ground motion. We will consider a generic formulation of F_{res} as a function of the longitudinal speed as follows:

$$F_{res} = k_0 + k_1 v_x + k_2 v_x^2$$

- a, b_f, and b_r are geometric relationships as shown in Figure 1;
- δ is the nose gear steering angle.

Tire model

In a generic tire model, the longitudinal and lateral forces are functions of the tire slip, i.e. the relative velocity of the tire tread with respect to the ground. Although the exact definitions vary among the tire models featured in literature, in most cases a side slip angle α and a longitudinal slip σ_x are defined as follows:

$$\alpha = \arctan\frac{v_{yw}}{v_{xw}}$$
$$\sigma_x = \frac{v_{xw} - R\omega}{v_{xw}}$$

where v_{xw} and v_{yw} are the relative speeds between tire and ground in longitudinal (tangential) resp. lateral (axial) direction with regard to a wheel-fixed reference system; R is the wheel radius and ω is the wheel rotational speed. In particular for the nose gear wheel, the steering angle needs to be taken into account. The side slip angle α_f is: [8]

$$\alpha_f = \delta - \arctan\frac{b_f\dot{\psi} + v_y}{v_x}$$

In a generic tire model and neglecting side effects such as variation of vertical load, variation of tire-ground friction coefficient, and tire deformation, the tire forces are continuous functions of these two slip quantities:

$$F_x = F_x(\sigma_x, \alpha) \qquad F_y = F_y(\alpha, \sigma_x)$$

A detailed description of these functions depends on the tire models adopted and will not be dealt with here. For each wheel on the vehicle, the rotational speed should be added to the dynamic problem as an additional state:

$$J_R\dot{\omega} = M - F_{xw}$$

with J_R moment of inertia of the wheel and M the driving or braking moment acting on the wheel.

Model simplification

The dynamic model can be simplified for the purpose of this study. Firstly, $\sigma_x = 0$ is assumed for all tires, i.e. there is no tire longitudinal slip and the tires will not spin when accelerating or block when braking. Consequently, the tire rotational speeds become functions of the aircraft longitudinal speed and yaw rate. Taking the same radius R for left and right main gear wheel, their rotational speeds are:

$$\omega_l = \frac{v_x - a\dot{\psi}}{R} \qquad \omega_r = \frac{v_x + a\dot{\psi}}{R} \quad (2)$$

Also, the driving and braking moments are directly translated into longitudinal forces without any dynamics:

$$F_{xl} = \frac{M_l}{R} \qquad F_{xr} = \frac{M_r}{R}$$

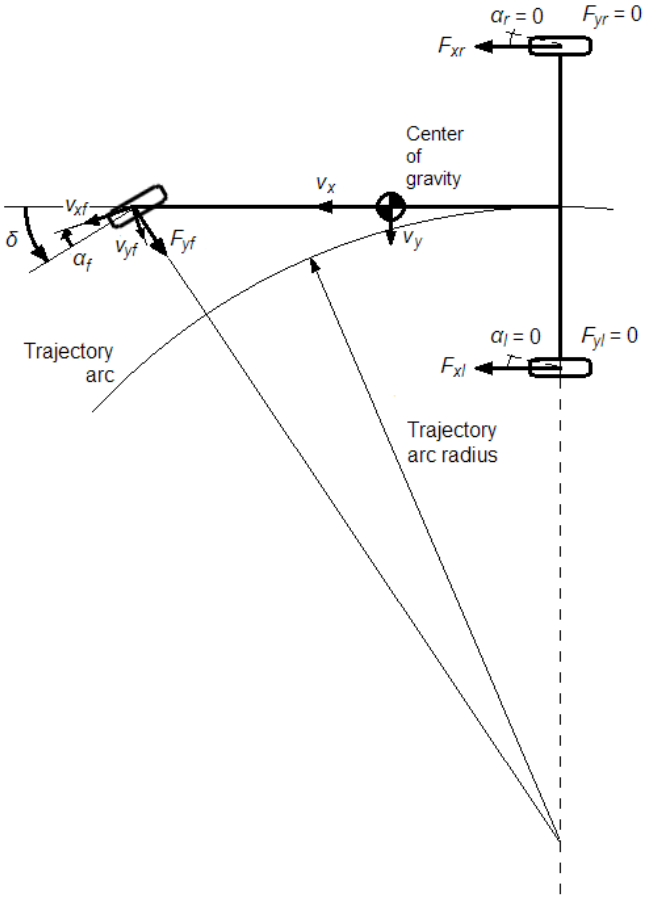

Figure 2. The assumption of zero slip angle on the main gear wheels results in a trajectory arc whose center lies on the prolongation of the main gear wheel axis.

Furthermore, the side slip angle of the main gear wheels is assumed to be zero at all times, which results in no lateral forces from the main gear tires. This assumption introduces an approximation which is negligible at low taxi speeds and implies that the center of the trajectory arc followed while cornering always lies on the prolongation of the axis of the main gear wheels (Figure 2). Also, the distance b_r is usually very short, meaning that the center of gravity lies near the crossing point of the aircraft longitudinal axis with the axis of the main gear wheels, i.e. the point where the trajectory arc is tangent to the aircraft longitudinal axis. For this reason, v_y turns out to be very small and can therefore be approximated to zero at all times.

A tire model is now only needed for the lateral behavior of the nose gear wheel. A simple linear model is taken here:

$$F_{yf} = k_f\alpha_f$$

where the constant coefficient k_f is called cornering stiffness in the tire dynamics literature.

In addition, all trigonometric functions are linearized by their first-degree Taylor approximation:

$$\sin x \approx x \qquad \cos x \approx 1 \qquad \arctan x \approx x$$

This is acceptable during standard taxi on a taxiway since the cornering radiuses are rarely smaller than approximately 50 m, which in turns means a steering angle δ not larger than approximately 10 degrees. It does introduce a noticeable error for tight maneuvers though, such as U-turns. The nose wheel side slip angle in its linearized form is:

$$\alpha_f = \delta - \frac{b_f \dot{\psi}}{v_x}$$

After these simplifications and substituting the expression for the nose wheel lateral force, the equations for the longitudinal and the yaw motion in Eq. 1 become in state-space form:

$$\begin{bmatrix} \dot{v}_x \\ \ddot{\psi} \end{bmatrix} = \begin{bmatrix} \frac{1}{m}\left[-k_f \left(\delta - \frac{b_f \dot{\psi}}{v_x} \right) \cdot \delta + \frac{1}{R}\left(M_l + M_r\right) - F_{res}\left(v_x\right) \right] \\ \frac{1}{J_z}\left[b_f k_f \left(\delta - \frac{b_f \dot{\psi}}{v_x} \right) + \frac{a}{R}\left(-M_l + M_r\right) \right] \end{bmatrix} \quad (3)$$

Note that despite the simplifications, this is still a nonlinear dynamic system with inputs δ, M_l, M_r and states v_x, $\dot{\psi}$.

Driving system model

The ground driving system includes the two electric motors, the energy storage, and one conventional carbon brake for each main landing gear.

Motor model

A detailed model of the motor dynamics is not needed for the purpose of this work. It is sufficient to consider a generic, direct current (DC) motor model and establish a relationship between the motor moment M and the motor root mean square (RMS) current i_{RMS}. In first approximation, neglecting effects such as magnetic saturation, a linear relationship holds with the constant coefficient C_M:

$$M = C_M i_{RMS} \quad (4)$$

In general, i_{RMS} is bounded by system constraints such as the maximum available power or the maximum motor current. When considering generator operation (regenerative braking), the negative limit on i_{RMS} is also a function of the momentary availability of the energy storage system. For instance, the storage system may be saturated or overheated, thus accepting only reduced or no input current. The time delay of the electric motors is several orders of magnitude smaller than the aircraft dynamics and can therefore be neglected for the scope of this work.

The thermal behavior of an electric motor is normally difficult to model with precision and strongly depends on the motor design; in fact, thermal aspects are one of the main drivers in the design of an electric machine. While specific thermal modeling is needed for a specific application involving a given motor type in order to analyze the heat exchange processes, we stick to the choice of a simplified DC motor model. In doing this, we neglect more complex phenomena given by specific system design features, such as inductance in an alternate current (AC) system, which may play a major role in influencing the efficiency of the motors. Normally, the thermal constraint on an electric motor is that a certain temperature should not be exceeded in order to avoid damage to the wirings or the magnetic elements (in the case of a permanent magnet motor). The main source of heat in the electric motor is assumed to be given by the copper losses, i.e. the electrical losses in the wirings, and losses due to electromagnetic effects. In general, they are a function of i_{RMS}^2. The thermal dissipation includes a conductive term dependent on the temperature and a term due to convection both around the motor housing and in the air gap of the motor. While convection is heavily influenced by the motor geometry and design, we assume that due to the needed power in the order of 100 kW per motor (see [7,9] for reference) a motor for the present application will probably require forced convection. [10] This can be realized, for example, by installing a fan on the rotor shaft forcing air into the motor air gap and/or around the motor. In this case, the convection heat transfer coefficient h is linearly dependent on the rotor speed. [11] Ultimately, the generic expression considered for the heat exchange in the motor is given by the following differential equation:

$$\dot{T} = w_w\left(i_{RMS}^2\right) - w_c\left(T - T_{amb}, \omega\right) \quad (5)$$

where T_{amb} is the ambient temperature (assumed constant), T is the temperature at a given critical point of the motor assembly where the temperature should be monitored, w_w is the heating contribution due to copper and electromagnetic losses (function of i_{RMS}^2), w_c is the cooling contribution due to heat conduction and convection and is assumed dependent on T-T_{amb} and the rotor speed ω. Note that the time dependency of the heat exchange is neglected here, although it does play a major role especially with heat conduction. However, such an analysis including solution of the heat equation and finite element modeling of an electric motor would go largely beyond the scope of the present work.

Energy storage model

An energy storage system accepts incoming currents from the motors working as generators or provides outgoing currents to supply the motors. This affects its State of Charge (SOC), a measure of the relative quantity of energy stored in the device. Such a system may be realized by means of batteries or supercapacitors; the technical nature of the system is however not relevant here. The energy storage system is modeled as a first order system with the following differential equation:

$$\dot{SOC} = \frac{dSOC}{dt} = \begin{cases} \eta_{\text{charge}} k_S i_S & \text{if } i_S > 0 \text{ and } SOC < SOC_{\max} \\ \eta_{\text{discharge}}^{-1} k_S i_S & \text{if } i_S < 0 \text{ and } SOC > SOC_{\min} \\ 0 & \text{otherwise} \end{cases} \quad (6)$$

where i_S is the current entering the storage system, k_S is a scaling coefficient and η_{charge} and $\eta_{\text{discharge}}$ are the efficiencies in the charging respectively discharging phase. Both efficiencies are in a range between 0 and 1 and η_{charge} will generally be smaller than $\eta_{\text{discharge}}$. Since more current is drawn from the battery than it flows into the motors in the discharge phase due to the efficiency smaller than 1, $\eta_{\text{discharge}}$ is inverted in eq. (6). This is not necessary with η_{charge} since less current will be supplied to the battery than it is generated by the

motors when charging. The current i_S is given by the sum of the motor RMS currents with changed sign:

$$i_S = -\left(i_{RMS,l} + i_{RMS,r}\right) \quad (7)$$

In order to transform (6) into a continuous function, the so-called logistic function is used:

$$S(x) = \frac{1}{1+e^{-\lambda x}} \quad (8)$$

This function, largely applied for instance in neural network theory, generates an S-shaped curve with an asymptotic value of 1 for large positive *x* and 0 for large negative *x*. The steepness of the transition from 0 to 1 in the vicinity of $x = 0$ is governed by the parameter λ. For sufficiently large λ, the logistic function well approximates a switching behavior between 0 and 1 when *x* changes sign. By introducing the logistic functions with *SOC* and i_S as arguments and appropriate parameters λ, Eq. 6 can be rewritten in an approximate form as follows:

$$\begin{aligned} \dot{SOC} = \quad & S(i_S)\cdot S(SOC_{\max} - SOC)\eta_{\text{charge}} k_S i_S + \\ & + S(-i_S)\cdot S(SOC - SOC_{\min})\eta_{\text{discharge}}^{-1} k_S i_S \end{aligned} \quad (9)$$

Each of the terms contains two logistic functions with different arguments. Due to the behavior of the logistic functions $S(i_S)$ and $S(SOC_{max}\text{-}SOC)$, the first term will approximately be zeroed if $i_S < 0$ or $SOC_{max}\text{-}SOC < 0$. Conversely, the logistic functions $S(-i_S)$ and $S(SOC\text{-}SOC_{min})$ will approximately zero the second term if $i_S > 0$ or $SOC\text{-}SOC_{min} < 0$. This results in a negated replication of the logic conditions stated in eq. 6. Depending on *SOC* and i_S, only the relevant term will remain in eq. 9 in the general case, resulting in a continuous approximation of the discontinuous function in eq. (6) (save for the errors due to the asymptotic behavior of eq. (8)).

Brake model

The carbon brakes are modeled as a moment input acting directly in the aircraft dynamic equations. The dynamics of the braking system are neglected.

Total model

The total dynamic model of the aircraft moving on ground with the electric driving system is now written by combining Eq. 2, Eq. 3, Eq. 4, Eq. 5 written for both motors (with subscripts *l* for left motor and *r* for right motor), and Eq. 9 and introducing the carbon brake moments M_{bl} and M_{br}:

$$\begin{bmatrix} \dot{v}_x \\ \ddot{\psi} \\ \dot{T}_l \\ \dot{T}_r \\ \dot{SOC} \end{bmatrix} = \begin{bmatrix} \frac{1}{m}\left[-k_f\left(\delta - \frac{b_f\dot{\psi}}{v_x}\right)\cdot\delta + \frac{C_M\left(i_{RMS,l}+i_{RMS,r}\right)}{R} - \frac{M_{bl}+M_{br}}{R} - F_{res}(v_x)\right] \\ \frac{1}{J_z}\left[b_f k_f\left(\delta - \frac{b_f\dot{\psi}}{v_x}\right) + \frac{aC_M\left(-i_{RMS,l}+i_{RMS,r}\right)}{R} + \frac{a\left(-M_{bl}+M_{br}\right)}{R}\right] \\ w_w\left(i_{RMS,l}^2\right) - w_c\left(T_l - T_{amb}, \frac{v_x - a\dot{\psi}}{R}\right) \\ w_w\left(i_{RMS,r}^2\right) - w_c\left(T_r - T_{amb}, \frac{v_x + a\dot{\psi}}{R}\right) \\ S(i_S)\cdot S(SOC_{\max} - SOC)\eta_{\text{charge}} k_S i_S + \\ \quad + S(-i_S)\cdot S(SOC - SOC_{\min})\eta_{\text{discharge}}^{-1} k_S i_S \end{bmatrix}$$

with $i_S = -\left(i_{RMS,l} + i_{RMS,r}\right)$ (10)

Writing state and input vectors explicitly:

$$\dot{\mathbf{x}} = \mathbf{f}(\mathbf{x},\mathbf{u}) \quad (11)$$

$$\mathbf{x} = \begin{bmatrix} v_x & \dot{\psi} & \dot{T}_l & \dot{T}_r & SOC \end{bmatrix}^T \qquad \mathbf{u} = \begin{bmatrix} \delta & i_{RMS,l} & i_{RMS,r} & M_{bl} & M_{br} \end{bmatrix}^T$$

Path Following Optimization

We consider the problem of driving the aircraft along a given trajectory while satisfying given performance objectives. It should be distinguished between *trajectory tracking* and *path following*. Trajectory tracking implies imposing desired trajectory parameters as a function of time, e.g. $\bar{v}_x(t), \bar{\dot{\psi}}(t)$, and controlling the aircraft so that it will follow them as closely as possible. In other words, the aim is to control the exact position of the aircraft at any given time instant. Path following instead deals with defining a desired trajectory that should be followed as closely as possible; however, time is an additional degree of freedom of the controller, i.e. the speed with which the trajectory is followed can be also optimized. Adapting the definitions in [12] to the present problem, we define the desired $\bar{v}_x(\vartheta), \bar{\dot{\psi}}(\vartheta)$ as functions of the path parameter $\vartheta(t) \in [\vartheta_0, \vartheta_1]$. Its time evolution $\dot{\vartheta}(t) = \upsilon$ is the additional degree of freedom of the optimization problem.

The strategy for calculating the optimal path following control is obtained by defining a cost function $C(\mathbf{x},\mathbf{u},\vartheta,\upsilon)$ and solving the optimal control problem:

$$\underset{\mathbf{u},\upsilon}{\text{minimize}}\; C(\mathbf{x},\mathbf{u},\vartheta,\upsilon) \quad (12)$$

subject to the system dynamic model:

$$\dot{\mathbf{x}} = \mathbf{f}(\mathbf{x},\mathbf{u}) \quad (13a)$$

as well as constraints on the inputs and constraints on the states such as temperature limitations:

$$\begin{aligned} & \delta \in [\delta_{\min}, \delta_{\max}], \\ & i_{RMS,l}, i_{RMS,r} \in [i_{RMS,\min}, i_{RMS,\max}] \\ & T_l, T_r \le T_{\max} \end{aligned} \quad (13b)$$

Also, constraints on the path parameter are needed, i.e. its starting point for t=0; its time evolution should be strictly positive to guarantee that the path is followed entirely in a finite

time; and the end of the path should be reached within a maximum time t_1:

$$\begin{aligned} &\vartheta = \vartheta_0 \text{ for } t = 0 \\ &\dot{\vartheta} = \upsilon > 0 \\ &\vartheta = \vartheta_1 \text{ for } t = t_1 \end{aligned} \quad (13c)$$

The main aspect in the setup of this problem is the definition of the cost function. The most important objective is the minimization of the path-following error. This part of the cost function will be:

$$C_e = \int_{t=0}^{t_1} \|\mathbf{e}(t)\| d\tau \qquad \text{with } \mathbf{e}(t) = \begin{bmatrix} \bar{v}_x(\vartheta(t)) - v_x(t) \\ \dot{\bar{\psi}}(\vartheta(t)) - \dot{\psi}(t) \end{bmatrix} \quad (14)$$

At the same time, the energy cost should be minimized. In this application, the objective should be to use the stored energy as often as possible when driving the aircraft and only resort to a primary energy source, e.g. the APU generator, if the stored energy is not available. In economic terms, this means that the energy coming from the storage system is free, while the energy coming from the primary source is costly. The proposed strategy is to use a linearly decreasing function of (SOC_{max}-SOC) as the energy cost that should only consider negative currents i_S (outgoing from the storage). In order to keep the cost function continuous, the logistic function of Eq. 8 is used again here. The part of the cost function for the driving case is then:

$$C_d = \int_{t=0}^{t_1} (SOC_{\max} - SOC) \cdot S(-i_S) \cdot i_S^2 d\tau \quad (15)$$

According to the same principle, carbon brakes should be used to decelerate only when it is not possible to brake with the electric motors and store energy. In other words, regenerative braking should be free while conventional braking should be costly. In this case, the proposed cost factor for regenerative braking is a linearly increasing function of (SOC-$SOC_{\min}$). The cost factor for conventional braking should be slightly lower than ($SOC_{\max}$-$SOC_{\min}$), so that when SOC approaches $SOC_{\max}$ the algorithm finds more convenient to use conventional braking. A factor of 0.95 is used for this. Again, the logistic function is used in order to have a continuous cost function. The cost function for the braking case is then:

$$C_b = \int_{t=0}^{t_1} \left[(SOC - SOC_{\min}) \cdot S(i_S) \cdot i_S^2 + 0.95 \cdot (SOC_{\max} - SOC_{\min}) \cdot (M_{bl} + M_{br}) \right] d\tau \quad (16)$$

Finally, the motor temperatures need to be kept low. The constraint on the temperatures in Eq. 13b ensures that they do not exceed the operating limit, but generally trying to keep the motors cool is beneficial for the wear and the availability of the system also in subsequent ground operations after the current trajectory planning. This also results in a contribution to the cost function which is proposed as a linear function of both motor temperatures:

$$C_T = \int_{t=0}^{t_1} (T_l + T_r) d\tau \quad (17)$$

The overall cost function is the weighted sum of Eq. 14, 15, 16, and 17:

$$C = \eta_e C_e + \eta_d C_d + \eta_b C_b + \eta_T C_T \quad (18)$$

By means of the weights η_e, η_d, η_b, η_T it is possible to regulate the relative importance of the cost function terms.

Additional considerations

All the conditions presented up to this point do not ensure time optimality in general. The time to completion of the trajectory can be considered with another term in the cost function if needed, although this will generally worsen the energetic efficiency.

By using Eq. 7 for calculating the total amount of current going to and from the storage system, the difference in motor resp. braking moments affecting the yaw motion is not considered. In a real system, even when one side decelerates by regenerative braking and the other side accelerates by the same amount and v_x is kept constant at the same time, because of the energetic losses the two currents will not be equal, but some current needs to be drawn from the energy sources. This is not taken into account in the present configuration. A controller based on this optimal path following can treat this effect as a disturbance on the yaw motion and correct the commands accordingly.

Using the steering system to produce yaw moment causes a resistance on the longitudinal motion, as can be seen in the first term of the equation for v_x in Eq. 10. Because the optimal control problem tends to minimize the motor currents, most of the yawing moment will be produced by differential moments rather than by using the steering system in this configuration as long as other constraints, e.g. the motor temperatures, do not oppose using the motors. In this situation, the steering system will be kept in the position of minimal wheel slip angle.

Preliminary optimization results

The result of some optimization simulations is presented here. The ACADO toolkit [13] has been used for this purpose. This is an open-source software environment for dynamic optimization and generation of optimized controllers. It features a Matlab interface that converts a dynamic system description from a user-friendly Matlab m-file-like language into self-contained C++ code for simulation. With regard to this work, ACADO is convenient in that it is capable of handling nonlinear dynamic systems and the generated C++ code may be used as core of a Model Predictive (MPC) controller in future stages of this project by using existing tools in the ACADO package or possibly even generating new tools thanks to its open-source status.

Due to numerical issues hindering the convergence of the optimization algorithm, only a subset of the cost function terms could be tested in the simulations. Also, the thermal equations of the electric motors are left out from the implemented model and conventional carbon braking is not applied. Furthermore, the transformation from motor moments to currents (see Eq. 4) is not performed, leaving the motor moments explicitly as in

Eq. 3. For a better understanding of the effects of the inputs, the dynamic system has been slightly changed by using a linear combination of M_l and M_r as new inputs:

$$M_{sum} = M_l + M_r \qquad M_{diff} = -M_l + M_r \quad (19)$$

The new input M_{sum} is thus the contributor to the longitudinal dynamics, whereas M_{diff} is the contributor to the yaw dynamics.

Two trajectories have been tested. In the first trajectory, the aircraft is accelerated and decelerated so that the longitudinal displacement, i.e. the integral of v_x, goes from 0 at start to 10 m at the end. The speed v_x should be zero both at start and at the end while $\dot{\psi}$ is kept zero at all times. At start, the storage system is at 80% of its maximum capacity. Figure 4 and Figure 5 show the results of two simulations. In the first simulation, the cost function is simply the squared driving moment:

$$C = \int_{t=0}^{t_1} M_{sum}^2 d\tau \quad (20)$$

The minimization of this cost function results in the least possible overall amount of energy to follow the trajectory. The speed v_x shows a parabolic, symmetric shape. In the second simulation, the cost function is a function of the driving moment and SOC:

$$C = \int_{t=0}^{t_1} [M_{sum} \cdot (SOC_{\max} - SOC)] d\tau \quad (21)$$

This cost function has a behavior that approximates Eq. 15 and 16 combined. A driving (i.e. positive) moment has a higher cost when SOC is low, while the lower SOC is, the more a braking (i.e. negative) moment will lower the overall cost. When starting the simulation with $SOC = SOC_{\max}$, the expected result of using this cost function is that because higher driving moments are favored, a longer acceleration up to a higher cruising speed will be commanded at the beginning of the trajectory compared to the first cost function in Eq. 20, thus ultimately reaching the end of the trajectory faster. While the algorithm did not reach convergence upon the last iteration, the tendency to command higher moments in absolute value can clearly be seen from the diagram in Figure 5. Because SOC was high at start, accelerating the aircraft more results in a reduction of the overall cost. Braking is also stronger because the cost function rewards energy regeneration. The maximum speed v_x reached is accordingly higher (Figure 4). However, the large acceleration occurs towards the end of the simulation and just before slowing down again, which does not appear sensible from an energetic point of view and does not meet the expectation of a faster travel along the whole trajectory (Figure 3). Further investigation is needed to determine whether this is due to the bad convergence of the algorithm or the cost function in the form of Eq. 21 does generally not provoke the expected behavior.

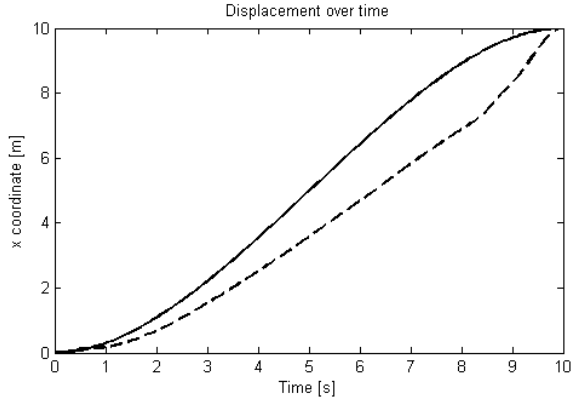

Figure 3. Longitudinal displacement over time for tracking of straight trajectory. Solid line: simulation with cost function based on driving moment. Dashed line: simulation with cost function based on driving moment and State of Charge.

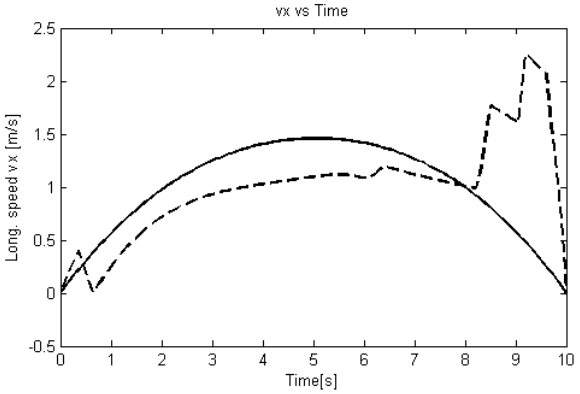

Figure 4. Longitudinal speed over time for tracking of straight trajectory. Solid line: simulation with cost function based on driving moment. Dashed line: simulation with cost function based on driving moment and State of Charge.

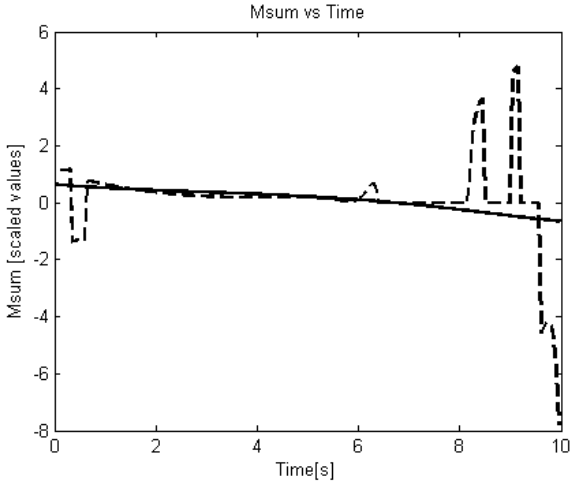

Figure 5. Driving moment over time for tracking of straight trajectory. Solid line: simulation with cost function based on driving moment. Dashed line: simulation with cost function based on driving moment and State of Charge. Note that the values in ordinates are scaled and dimensionless.

The second trajectory is a 90 degree corner at a speed vx = 10 m/s that must be kept constant during the whole simulation. The cost function is the squared driving moment (Eq. 20), which is expected to indirectly increase the contribution of M_{diff} and decrease that of δ in generating yaw moment. Figure 6 shows the yaw rate of the aircraft as a result of the controlled movement along the commanded trajectory. The driving moment and yaw moment commands can be seen in Figure 7, whereas the steering angle command is shown in Figure 8. Again, the algorithm could not reach the full convergence upon the last iteration. Figure 9 shows the comparison between commanded trajectory and simulated trajectory, while Figure 10 displays the lateral error along the trajectory, which ranges between -1.47 m and 1.61 m. It remains to be cleared to what extent this error is due to the lack of convergence rather than limitations in the model or other causes. Because different cost functions have not yet been tested, it is not possible at this stage to perform comparisons and further discuss the results for this case.

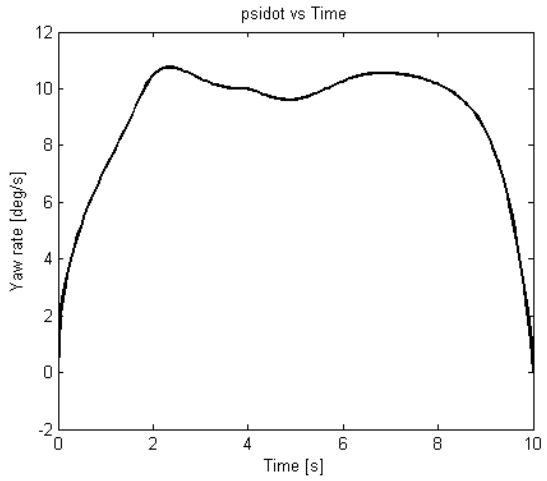

Figure 6. Yaw rate over time for tracking of cornering trajectory

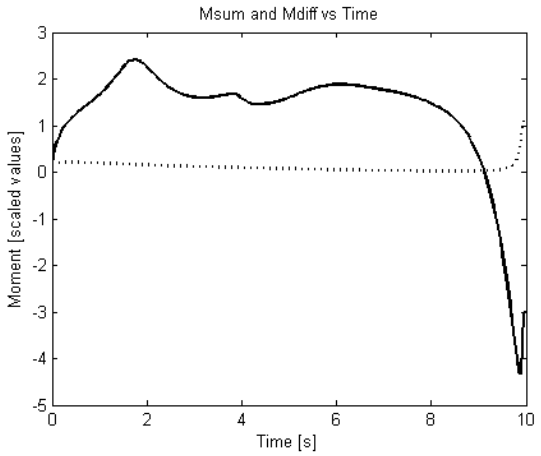

Figure 7. Driving moment M_{sum} (solid line) and yawing moment M_{diff} (dotted line) over time for tracking of cornering trajectory

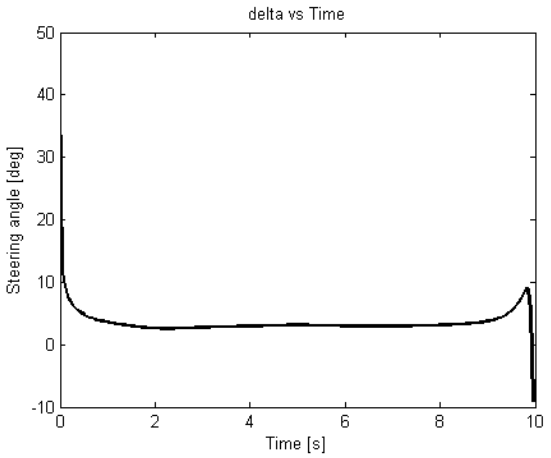

Figure 8. Steering angle over time for tracking of cornering trajectory

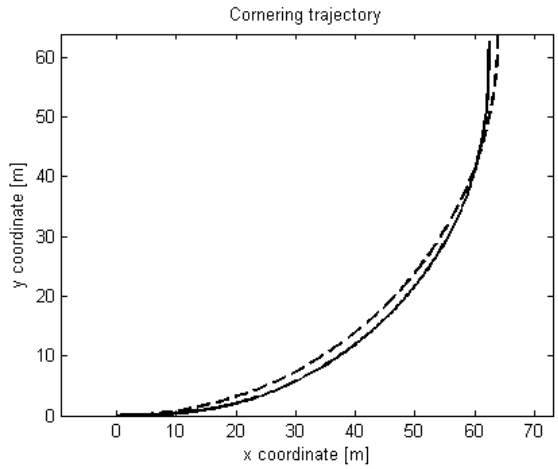

Figure 9. Commanded trajectory (dashed line) and simulated trajectory (solid line) in cornering simulation

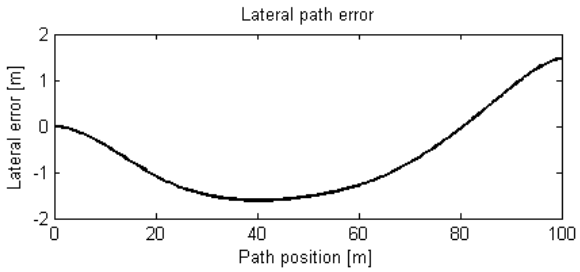

Figure 10. Lateral path error in cornering simulation

Summary and Outlook

In an effort to lower the overall fuel consumption and emissions of commercial flights, there has recently been a substantial interest in low- or zero-emission ground propulsion technologies. Especially, systems featuring electric motors in the landing gears have been proposed. An aircraft equipped with such a system is overactuated in its ground motion. Therefore, a control allocation strategy is required to follow a

prescribed trajectory. In this paper, such a strategy has been proposed starting from the analysis of the system dynamics. The optimizing strategy is based on minimization of a cost function subject to the nonlinear dynamic system of the aircraft on ground. While the main driver is the energetic efficiency, constraints such as motor temperatures are also considered. Preliminary simulations showed the behavior of the optimization strategy in selected, simplified situations. It was clear that numeric aspects are key for a successful convergence of the optimization algorithm. This and the convergence speed of the optimization are vital aspects in order to use the algorithm in a Model Predictive Control (MPC) scheme. Further effort should be put into this aspect in the future steps of this research topic. Among the directions to explore, it should be investigated if linearized models can lead to satisfactory results with little approximation error. Given the strongly nonlinear nature of the system, gain scheduled MPC might be an interesting option to obtain a good control precision over the whole operating range. Ultimately, the question to answer is whether MPC, by predicting the future system states, is able to produce a substantially better control strategy than simpler controllers. Since the thermal behavior of the motors and the storage system capacity have a sensibly slower dynamics than the aircraft motion, “looking into the future” with MPC might better exploit the characteristics of the prescribed trajectory and eventually make the most of the system for the best possible energetic efficiency.

References

1. Schürmann, Schäfer, Jahn, Hoffmann, Bauerfeind, Fleuti, and Rappenglück, “The impact of NOx, CO and VOC emissions on the air quality of Zurich airport“, *Atmospheric Environment*, vol. 41, pp. 103-118, 2007. DOI:10.1016/j.atmosenv.2006.07.030
2. Graham, “Managing Airports: An international perspective”, 3rd ed., Butterworth-Heinemann, 2008.
3. “Sesar Definition Phase - Deliverable D1 - Air Transport Framework,The Current Situation,” July 2006.
4. Bureau of Transportation Statistics Special Report, “Sitting on the Runway: Current Aircraft Taxi Times Now Exceed Pre-9/11 Experience”, U.S. Department of Transportation Research and Innovative Technology Administration, May 2008.
5. Deonandan and Balakrishnan, “Evaluation of Strategies for Reducing Taxi-out Emissions at Airports,” in *Proceedings of the AIAA Aviation Technology, Integration, and Operations (ATIO) Conference*, September 2010.
6. Airbus Customer Services Manual, “Flight Operations Support & Line Assistance: Getting to Grips with Fuel Economy,” July 2004.
7. Re, “Viability and State of the Art of Environmentally Friendly Aircraft Taxiing Systems,” *International Conference for on Electrical Systems for Aircraft, Railway and Ship Propulsion (ESARS),* Bologna, Italy, October 16th-18th, 2012. DOI 10.1109/ESARS.2012.6387462
8. Isermann: Fahrdynamik-Regelung. ATZ/MTZ-Fachbuch. Vieweg+Teubner (2006)
9. Re, "Assessing Environmental Benefits of Electric Aircraft Taxiing through Object-Oriented Simulation," SAE Int. J. Aerosp. 5(2):503-512, 2012. DOI:10.4271/2012-01-2218
10. Raminosoa, Hamiti, Galea, and Gerada, “Feasibility and Electromagnetic Design of Direct Drive Wheel Actuator for Green Taxiing,” in IEEE Energy Conversion Congress and Exposition, 2011.
11. Staton and Cavagnino, “Convection Heat Transfer and Flow Calculations Suitable for Electric Machines Thermal Models”, IEEE Transactions on Industrial Electronics, vol. 55, no. 10, October 2008.
12. Faulwasser, Kern, and Findeisen, “Model Predictive Path-Following for Constrained nonlinear Systems”, Joint 48th IEEE Conference on Decision and Control and 28th Chinese Control Conference, Shanghai, P.R.China, December 16-18, 2009.
13. Houska, Ferreau, and Diehl, “ACADO Toolkit – An Open-Source Framework for Automatic Control and Dynamic Optimization”, Optimal Control Applications and Methods, vol. 32 no. 3, 298-312, 2011.

Contact Information

Fabrizio Re
DLR German Aerospace Center
Institute of System Dynamics and Control
Muenchner Strasse 20
82234 Wessling
Germany